



HAL
open science

Corrosion-fatigue behaviour of Cr–Mo steel under biaxial tension

Vidit Gaur, Véronique Doquet, Emmanuel Persent, Eléonore Roguet

► **To cite this version:**

Vidit Gaur, Véronique Doquet, Emmanuel Persent, Eléonore Roguet. Corrosion-fatigue behaviour of Cr–Mo steel under biaxial tension. *Fatigue and Fracture of Engineering Materials and Structures*, 2020, 43 (11), pp.2560-2570. 10.1111/ffe.13276 . hal-02995567

HAL Id: hal-02995567

<https://hal.science/hal-02995567v1>

Submitted on 9 Nov 2020

HAL is a multi-disciplinary open access archive for the deposit and dissemination of scientific research documents, whether they are published or not. The documents may come from teaching and research institutions in France or abroad, or from public or private research centers.

L'archive ouverte pluridisciplinaire **HAL**, est destinée au dépôt et à la diffusion de documents scientifiques de niveau recherche, publiés ou non, émanant des établissements d'enseignement et de recherche français ou étrangers, des laboratoires publics ou privés.

1 ORIGINAL CONTRIBUTION

2 **Corrosion-fatigue behavior of Cr-Mo steel under biaxial tension**3 Vedit Gaur*¹ | Véronique Doquet² | Emmanuel Persent³ | Eléonore Roguet³

¹Department of Mechanical and Industrial Engineering, Indian Institute of Technology Roorkee, Roorkee 247667, India

²Laboratoire de Mécanique des Solides, CNRS UMR7649, Ecole Polytechnique Institut Polytechnique de Paris, 91128 Palaiseau, France

³IFP Energies Nouvelles, 1 et 4 avenue de Bois-Préau, 92852 Reuil-Malmaison, France

4 **Correspondence**

*Email: vedit.gaur@me.iitr.ac.in

Abstract

Combined cyclic tension and internal pressure tests with various proportions of each loading were run on a 2.5%Cr-1%Mo steel in air and in 3.5% NaCl solution, with and without cathodic protection to investigate the effect of positive stress biaxiality on corrosion-fatigue lives and damage mechanisms. At free potential, a strong reduction in fatigue resistance was observed for uniaxial as well as for equibiaxial cyclic tension, and attributed to multiple crack initiation from corrosion pits. Cathodic protection completely cancelled the detrimental effect of the corrosive environment on fatigue lives whatever the load biaxiality was, in spite of an obvious enhancement of intergranular fracture attributed to hydrogen embrittlement.

KEYWORDS:

Biaxial tension, Intergranular facets, Hydrogen embrittlement, Corrosion fatigue, Steel, Pits

5 **NOMENCLATURE**

| | |
|--|---|
| α | Crack tip constraint factor |
| B | Biaxiality ratio |
| C_0, C_H | Equilibrium concentration of hydrogen: in the stress-free metal, stressed metal |
| ΔF | Axial load range |
| ΔP | Internal pressure range |
| ΔK | Stress intensity factor range |
| e | Thickness of tubular specimen |
| R | Load or Stress ratio |
| R_a | Arithmetic average surface roughness |
| R_g | Universal gas constant |
| R_m | Mean radius |
| S | Cross-sectional area |
| $\sigma_1/\sigma_{xx}/\sigma_{\theta\theta}$ | Hoop's or Circumferential stress |
| σ_2/σ_{zz} | Axial or Longitudinal stress |
| σ_h | Hydrostatic stress |
| $\sigma_{min}, \sigma_{max}, \sigma_a, \Delta\sigma$ | Minimum, Maximum, Amplitude and Range of cyclic stress |
| T | Temperature |
| $\frac{T_x}{V_H}$ | Stress triaxiality ratio |
| V_H | Average molar volume of hydrogen |

1 | INTRODUCTION

The components of many structures are subjected to multiaxial cyclic loading in addition to environmental effects. In certain applications, like pressure vessels or components subjected to thermal fatigue, biaxial cyclic tension is encountered. Most of the studies on fatigue behaviour and crack growth are devoted to uniaxial loading. Less data is available on multiaxial loading, and most of it concerns combined tension and shear, rather than biaxial tension, partly because of the challenges involved in conducting cyclic biaxial tension tests. Biaxial tension can be applied to cruciform specimens loaded in two orthogonal directions^{1,2,3}, circular or elliptical plates submitted to biaxial bending^{4,5,6} and tubular specimens loaded in tension and internal pressure^{7,8}. The effect of biaxial tension on fatigue lives was reported to be beneficial^{9,10} or detrimental^{11,12} or neutral¹³ depending on the load biaxiality ratio. All these studies have however been conducted in ambient air, at room temperature, and very few studies on environmental effects on biaxial tension fatigue are available.

Corrosive environments deteriorate the fatigue resistance of most metals, often due to the nucleation of pits, their growth to a critical size allowing the initiation of short cracks, the growth of the microcracks in and around the pits, and finally their coalescence. Fracture mechanics is often used to analyse such a damage process^{14,15}. To the author's knowledge, the way cyclic biaxial tension influences corrosion pitting and the associated crack nucleation process has not been investigated so far.

To protect the metal surface from corrosion, a cathodic potential is generally applied, but a high negative cathodic potential can enhance hydrogen release and promote hydrogen-induced "embrittlement" through two main mechanisms: Hydrogen-enhanced decohesion¹⁶ or Hydrogen-enhanced localized plasticity¹⁷. Since the solubility and diffusivity of hydrogen are sensitive to the stress triaxiality ratio, a difference in corrosion-fatigue resistance of metals under cathodic protection might be expected between uniaxial and biaxial tension loading.

However, nearly all the corrosion-fatigue studies done so far involved uniaxial loading, and only a handful of data is available for biaxial tension^{13,18,19}. These studies investigated the effect of the load biaxiality ratio ($B = \frac{\sigma_2}{\sigma_1} = 0,1$ or 1.5) on fatigue crack growth in 2024-T3, 7075-T6 and 5083-H116 aluminium alloys in salt water. For 7075-T6 alloy, an enhanced detrimental effect of equibiaxial tension was observed in the Paris regime in salt water, but no effect in the near threshold regime, while for 2024-T3 alloy, the detrimental effect of load biaxiality was observed in the near threshold regime only^{18,13}. Perel et al.¹⁹ also reported a detrimental effect of load biaxiality on crack growth rates in 5083-H116 aluminium alloys in salt water. The influence of load biaxiality on corrosion-fatigue seems thus very dependent on the material, and has not been investigated in steels so far.

The present study thus contributes to fill this gap. This work is motivated by corrosion-fatigue issues in offshore oil drilling structures, more specifically "Clip-RiserTM connectors" designed at IFPEN to connect/disconnect conveniently the riser tubes. When immersed in sea water, the assembly not only experiences external pressure from sea water but also the internal pressure of oil flowing through it as well as the weight of the riser assembly, buoyancy force, and sea waves and currents, which induce cyclic bending with a random amplitude. Finite element computations have shown that the component undergoes in-phase biaxial cyclic tension at certain critical locations, in addition to the environmental effect.

The effects of load biaxiality on fatigue lives and damage mechanisms in air of the steel which constitutes the Clip-RiserTM connectors were thus investigated and reported in two previous papers^{20,21}. The present paper focusses on the combined effects of load biaxiality and the corrosive environment. Combined cyclic tension and internal pressure tests with various proportions of each loading were run on tubular specimens in 3.5% NaCl solution, with or without any cathodic protection. The later enhances the evolution of hydrogen, and thus its ingress into the metal, thereby enabling us to investigate, through fractographic observations, how the deleterious effects of hydrogen on fatigue damage are modified by biaxial loading.

2 | EXPERIMENTAL STUDY

2.1 | Material characterization

The material constituting the Clip-RiserTM connector is 2.5%Cr-1%Mo steel with the chemical composition shown in Table 1, as per the ASTM standard A182. The material was water-quenched after austenitization between 940°C and 970°C and finally tempered at 625°C. The material is a non-textured, aged martensite, with nearly equiaxed austenitic grain size of 6.5 μm to 7.7 μm . Several inclusions of an average size of 5 μm are present along with some less frequent but large pores and inhomogeneities (40 – 300 μm) (Figure 1). The detailed microstructural and texture analysis and the effect of these inclusions, pores or inhomogeneities on fatigue damage mechanisms in this material under different loading conditions has been discussed in previous

papers^{20,21}. Tensile tests were conducted on cylindrical specimens, 8 mm dia, at a constant strain rate of 10^{-3} /sec. The measured tensile properties are shown in Table 2.

2.2 | Experimental Procedures

Tubular specimens (Figure 2) of outer diameter 25 mm, thickness $e = 1$ mm and internal/external surface roughness, R_a , of $0.2 \mu\text{m}$ were used for load/pressure-controlled, in-phase tension and internal oil pressure tests. A triaxial testing machine ($\pm 100\text{kN}$, $\pm 600\text{Nm}$, 1500 bars) was used for all the fatigue and corrosion-fatigue tests. The tests in air were run at 10 Hz, while those in salt water were run at 4 Hz, using sinusoidal waveform at a constant load/stress ratio ($R = \sigma_{\min}/\sigma_{\max} = 0.25$). A prior study at IFPEN had shown no observable difference between 1 Hz and 4 Hz.

For the corrosion-fatigue tests, a setup (shown in Figure 3) was designed in-house and coupled with the fatigue machine. The specimen was enclosed in a PMMA (Polymethyl methacrylate) chamber filled with 3.5% NaCl solution, which was circulated via a circulation pump connected to a 5L reservoir of solution. A volume of 100 mL of solution per cm^2 of exposed surface of the specimen was maintained. An aeration pump was used to continuously produce bubbles in the reservoir so as to keep the solution saturated in oxygen. In actual conditions of Clip-RiserTM connector, the dissolved oxygen depends on the depth, water temperature, salinity and organic material content. A mean temperature of around 22°C with slight deviation of $\pm 3^\circ\text{C}$ and a mean pH of 7.2 with deviation of ± 0.5 was measured for the solution in the reservoir, which is acceptable. The solution was renewed after each test.

For the application of a cathodic potential, a digital potentiostat was used along with a reference electrode (Ag/Ag^+) and a counter electrode (Platinum electrode). A potential of -950 mV was applied. This value is sufficiently negative to ensure a substantial release of hydrogen gas around the specimen, and to study its effects on the fatigue behavior of this steel.

The axial load amplitude ΔF and pressure amplitude ΔP were chosen so as to get the desired biaxiality ratio (B), defined as:

$$B = \frac{\Delta\sigma_{\theta\theta}}{\Delta\sigma_{zz}} = \frac{\frac{\Delta PR_m}{e}}{\frac{\Delta F}{S} + \frac{\Delta PR_m}{2e}} \quad (1)$$

where R_m is the mean radius and S the cross section of the tubes. The consistency of expected and measured stress states within the gage length of the specimen were checked using strain gage rosettes. The fatigue tests were performed under uniaxial ($B = 0$) and equibiaxial ($B = 1$) loading conditions, at a fixed load ratio, $R = 0.25$, in free corrosion or with cathodic potential. An additional biaxiality ratio of $B = 0.25$ was investigated for the tests with cathodic potential. The tests were run until a through crack with complete separation (for $B = 0$) occurred, or an oil leakage (for $B = 1$ and 0.25) was detected, or till the specimen ran-out for 2×10^6 cycles.

The fracture surfaces of the broken specimen were examined using Scanning Electron Microscopy (SEM). The corroded surfaces were first cleaned using a solution of 3.5 g of hexamethylene tetramine (HMTA) in 500 mL of hydrochloric acid (specific gravity of 1.19). Hydrochloric acid being reactive could do some etching to sample but the extent of etching was insignificant. A digital optical microscope was used to perform topographic measurements.

3 | RESULTS

3.1 | Biaxial tension fatigue in air

The results of biaxial tension fatigue tests done in air at various biaxiality ratios were already discussed in previous papers^{20,21}, and are only briefly reported here, in Table 3 and Figure 4. Compared to uniaxial loading, the fatigue resistance of the material was slightly enhanced at low biaxiality ratio ($B = 0.25$) but slightly reduced by equibiaxial tension ($B = 1$). Von-Mises equivalent stress range is a non-linear function of B , which decreases from $\Delta\sigma_{zz}$ for $B = 0$, to $0.90\Delta\sigma_{zz}$ for $B = 0.25$, and down to a minimum value of $0.87\Delta\sigma_{zz}$ for $B = 0.5$, before going up to $\Delta\sigma_{zz}$, for $B = 1$. However, Von-Mises equivalent stress range does not rationalize the observed behavior. Surface-cutting defects were responsible for most crack initiations, and the stress concentration factor, K_t , near a surface semi-spherical pore was thus computed, and found to decrease as load biaxiality increases: $K_t = 2.04$ for $B = 0$, 1.90 for $B = 0.25$, and 1.64 for $B = 1$. Biaxial tension should thus delay crack initiation from surface-cutting pores, which can explain the beneficial effect of a small biaxiality ratio. In spite of that, equibiaxial loading had a detrimental effect, which was attributed to a pseudo size effect. In high cycle fatigue, life is, to a large extent, controlled by the number of cycles needed for microcracks to cross the first grain boundaries that they encounter, which depends upon the relative

misorientations of the grains. Thus, the Fatigue life depends on the presence of moderately misoriented grains along the first principal plane, on each side of a grain favorably orientated for cyclic plasticity and crack nucleation. Under equibiaxial tension, there are two equivalent principal planes, so that the probability to find a cluster of suitably oriented grains along those two planes should be twice as high. Transverse cracks initiating from inner or outer surface of the tubular specimen were observed for uniaxial loading, while for equibiaxial tension, both longitudinal and transverse cracks were observed, and sometimes initiated from the inner surface.

The fracture surfaces exhibit a mixture of inter-granular and trans-granular areas with a surface fraction of inter-granular facets very much dependent on ΔK , as reported and discussed in previous article²¹. This fraction first increases with ΔK until it reaches a maximum around 40-45% for $\Delta K \approx 10 \text{ MPa}\sqrt{\text{m}}$, and then it decreases down to zero for $\Delta K \approx 15 \text{ MPa}\sqrt{\text{m}}$. Such facets are known to result from a combination of temper and hydrogen embrittlement of the grain boundaries^{22,23,24,25}, since their formation was shown to require both a segregation of impurities during the heat treatment, and hydrogen release by a reaction of water vapor with the metal at the crack tip, during fatigue crack growth.

3.2 | Biaxial corrosion fatigue without cathodic potential

The results of corrosion-fatigue tests at free potential for different load biaxiality ratios are reported in Table 4. Figure 4 compares the evolutions of fatigue lives with the amplitude of the maximum principal stress for two biaxiality ratios ($B = 0$ and 1) in air, and in salt water.

In air, equibiaxial loading was slightly detrimental, compared to uniaxial loading, while in salt water, the fatigue data at $B = 0$ and $B = 1$ nearly followed the same trend, with a strong reduction in fatigue resistance in both cases, compared to air, and a suppression of the endurance limit. In other words, the detrimental effect of equibiaxial tension was not enhanced by salt water at free potential.

All fatigue failures in salt water initiated from the outer surface, exposed to the solution. Optical observations of specimen's outer surface after corrosion-fatigue tests revealed the presence of multiple corrosion pits (Figure 5a). 3D optical imaging of the (Figure 5b) was used to measure their surface radius and depth. The average depth-to-radius ratio of the pits in uniaxial tension was 0.33 ± 0.3 , while in biaxial tension it was 0.31 ± 0.2 . Images of the specimen's outer surfaces were captured at the same magnification after uniaxial or biaxial corrosion-fatigue, and the number of pits per unit surface was determined. The density of pits after uniaxial corrosion-fatigue was approximately $2.7/\text{mm}^2$, while it was $3.1/\text{mm}^2$ after equibiaxial corrosion-fatigue. Thus, biaxial loading does not seem to influence much the aspect ratio and the density of pits, as compared to uniaxial tension.

Most of the cracks initiated from the bottom of such corrosion pits (Figure 5). The stress concentration there was thus high enough to overcome the gradient of hoop stress through the thickness of the specimen ($\sigma_{\theta\theta}$ is 8% higher on the inner surface), thus favouring crack initiation from the exposed surface. For $B = 1$, cracks initiated in random orientation without any preference for the longitudinal or transverse direction, contrary to what was observed in air (see Table 4 and Figure 6a). In some cases, the coalescence of small cracks were also observed (Figure 6b).

For uniaxial loading, the fracture surfaces showed crystallographic patterns evoking trans-granular brittle decohesion (Figure 7a), with very few inter-granular facets, while for equibiaxial loading, trans-granular decohesion was also observed, but inter-granular facets were predominant (Figure 7b).

3.3 | Biaxial tension corrosion fatigue with cathodic potential

Corrosion-fatigue tests were also run at three different biaxiality ratios ($B = 0, 0.25$ and 1) with a cathodic potential of -950 mV . The test results are reported in Table 5. Figure 8 shows the evolution of the fatigue lives with the maximum stress amplitudes for the three biaxiality ratios, compared with the data obtained in air. In these conditions, the fatigue lives remained unaltered as compared to those in air. Figure 9 compares the surface conditions of two specimens as seen under optical microscope after fatigue tests run in salt water with or without cathodic protection. In free corrosion without cathodic potential, the surface was corroded (formation of pits), while the cathodic protection prevented the specimen from being corroded. As a consequence, like in air, cracks initiated from the inner (unexposed) surface as well as from the outer (exposed) surface of the specimen (see Table 5). For low biaxiality ratios ($B = 0$ and 0.25), crack initiated in transverse direction, while for equibiaxial loading ($B = 1$) crack initiated in longitudinal or transverse directions (and not randomly, as at free potential).

Figure 10 compares fracture surfaces formed in air and in salt water with cathodic protection at nearly the same ΔK . In air, the fracture surface was mixed: intergranular and transgranular with no more than 50% intergranular facets, while in salt water

143 with cathodic protection, the fracture surface was totally intergranular (and this was also the case along the whole crack path)
144 irrespective of the biaxiality ratio.

145 4 | DISCUSSION

146 The biaxial fatigue tests run in environmental and mechanical conditions representative of in-service conditions for Clip-Riser™
147 connectors, have shown that the detrimental effect of environment is not enhanced by the load biaxiality. For design purposes,
148 the effects of load biaxiality and of corrosion can thus be considered separately.

149 In corrosion-fatigue with cathodic protection, the fracture surfaces were fully inter-granular (Figure 10b) irrespective of
150 investigated biaxiality ratios ($B = 0, 0.25$ and 1), while the fraction of inter-granular facets never exceeded 50% in air. The
151 enhancement of inter-granular fracture when applying a sufficiently negative cathodic potential to ensure the release of hydrogen
152 in the solution is consistent with the interpretation of such fracture as a sign of combined temper and hydrogen embrittlement.
153 The absence of any associated reduction in fatigue lives compared to the tests run in air suggests either that crack propagation
154 constituted only a small fraction of the fatigue lives, or that the material already underwent such a substantial hydrogen-induced
155 embrittlement in air that the enhancement of this effect by cathodic potential only had a marginal impact in terms of crack growth
156 rate. A third explanation might be a rise in asperity-induced crack closure effects when crack propagation becomes fully inter-
157 granular. Oriani et al.²⁶ proposed a relation suggesting the role of hydrostatic stress in assisting the diffusion of the hydrogen
158 atoms in a metal:

$$C_H = C_0 \exp \frac{\sigma_H \overline{V}_H}{R_g T} \quad (2)$$

159 Where C_H is the equilibrium concentration of hydrogen in stressed metal, C_0 is the equilibrium concentration in the stress-
160 free metal, σ_H is the hydrostatic stress, T is temperature, \overline{V}_H is the average molar volume of hydrogen in the metal and R_g is the
161 gas constant. According to this equation, an enhancement of hydrogen embrittlement effects by biaxial tension was expected.

162 Ritchie²³ related the intergranular fracture during fatigue crack growth in quenched and tempered steels to the high hydrostatic
163 tension ahead of the crack tip. It was suggested that inter-granular fracture is controlled by the stress triaxiality ratio ahead of
164 the crack tip:

$$T_x = \frac{\sigma_H}{\sigma_{eq}} \quad (3)$$

165 In order to estimate the effect of biaxial tension on stress triaxiality ahead of the deepest point of a surface crack in a tube, a
166 3D finite element model of 500 μm -deep semi-circular crack in a 10 mm-thick plate was developed using ABAQUS™ software.
167 For symmetry reasons, only 1/4th of the plate was considered. The mesh and the boundary conditions are shown in Figure 11.
168 C3D10 type tetrahedral quadratic elements with 4 integration points were used for far-field body, while C3D20R type reduced-
169 integration quadratic elements with 8 integration points were used for the crack front area. Far from the crack front, the mesh
170 size was 0.5 mm and it was continuously reduced to 5 μm close to the crack front. The latter mesh size was checked to be less
171 than 1/10th of the cyclic plastic zone size. Ten cycles of combined opening stress σ_{zz} and tensile stress parallel to the free surface
172 $\sigma_{xx}(= B\sigma_{zz})$ were simulated at $R = 0.25$ for $B = 0, 0.25, 0.5$ and 1 , using elastic-plastic constitutive equations with non-linear
173 isotropic and kinematic hardening previously identified based on experimental stress-strain loops at various strain ranges²⁰. The
174 applied loading range $\Delta\sigma_{zz}$, according to Newman & Rajus expressions²⁷, corresponded to $\Delta K_I = 10 \text{ MPa}\sqrt{\text{m}}$. This value was
175 chosen because it was found to yield the highest fraction of inter-granular facets²¹.

176 The comparison of the stress triaxiality profiles ahead of the deepest point at σ_{max} is shown in Figure 12a. Compared to
177 uniaxial loading ($B = 0$) biaxial loading increases the stress triaxiality ratio, but this increase is not very large. The comparison
178 of the crack opening displacement profiles behind the deepest point is shown in Figure 12b. Compared to uniaxial tension,
179 biaxial tension reduces crack tip blunting. A localized slip band allowing hydrogen transport by the dislocations to the grain
180 boundary is more likely to form at a sharp crack tip than at a blunt tip. This effect might counterbalance the effect of the weak
181 rise in stress triaxiality ratio.

182 Such opposite effects would also be consistent with the limited increase in fatigue crack growth rate in salt water reported
183 in^{18,19} for aluminum alloys under equibiaxial tension as compared to uniaxial tension.

5 | CONCLUSIONS

Biaxial corrosion-fatigue tests were conducted so as to mimic in-service conditions for Clip-Riser™ connectors, constituted of Cr-Mo steel, and subjected to multiaxial cyclic loadings in sea water. The tests were conducted at representative load biaxiality ratios, with and without cathodic potential, and based on the observed results, the following conclusions can be drawn

- At free potential, a strong reduction in fatigue resistance of 2.5%Cr-1%Mo steel was observed in salt water for uniaxial as well as for equibiaxial cyclic tension, with a disappearance of the endurance limit.
- The slight detrimental effect of equibiaxial tension observed in air was not enhanced by the corrosive environment at free potential.
- For design purposes, the effects of load biaxiality and of corrosion can thus be considered separately.
- Multiple crack initiation from corrosion pits was the main cause of the deleterious effect of salt water at free potential.
- Load biaxiality did not significantly modify the size and surface density of corrosion pits.
- Cathodic protection completely cancelled the detrimental effect of corrosive environment on fatigue lives, whatever the load biaxiality, in spite of an obvious enhancement of inter-granular fracture attributed to hydrogen embrittlement.

6 | ACKNOWLEDGMENTS

Authors are thankful for M. Jean Kittel (IFPEN, Solaize) for his kind support during the experimental work for the corrosion setup and analysis in this study and to IFEPN for funding this study.

References

1. Bonnard V., Chaboche J.L., Gomez P., Kanouté P., Pacou D.. Investigation of multiaxial fatigue in the context of turboengine disc applications. *International Journal of Fatigue*. 2011;33:1006-1016.
2. Sunder R., Ilchenko B. V.. Fatigue crack growth under flight spectrum loading with superposed biaxial loading due to fuselage cabin pressure. *International Journal of Fatigue*. 2011;33(8):1101-1110.
3. Lee E.U., Taylor R.E.. Fatigue behavior of aluminum alloys under biaxial loading. *Engineering Fracture Mechanics*. 2011;78(8):1555 - 1564.
4. Kane A., Doquet V.. Surface crack and cracks networks in biaxial fatigue. *Engineering Fracture Mechanics*. 2006;73(2):233-251.
5. Koutiri I., Bellett D., Morel F., Augustins L., Adrien J.. High cycle fatigue damage mechanisms in cast aluminium subject to complex loads. *International Journal of Fatigue*. 2013;47:44-57.
6. Kamaya M., Tsuji T.. Evaluation of equi-biaxial fatigue of stainless steel by the pressurized disc fatigue test. *International Journal of Fatigue*. 2014;61:107-115.
7. Marquis G., Karjalainen-Roikonen P.. Long-life multiaxial fatigue of SG cast iron. In: Proc. 6th International Conference on Biaxial/Multiaxial loading and Fracture; 2001; 151-159.
8. Itoh T., Fukumoto K., Hagi H., Itoh A., Saitoh D.. Low Cycle Fatigue Damage of Mod.9Cr-1Mo Steel under Non-Proportional Multiaxial Loading. *Procedia Engineering*. 2013;55:457-462.
9. Doquet V., De Greef V.. Dwell fatigue of a titanium alloy at room temperature under uniaxial or biaxial tension. *International Journal of Fatigue*. 2012;38:118-129.

- 219 10. Bellett D., Morel F., Morel A., Lebrun J.-L.. A Biaxial fatigue specimen for uniaxial loading. *Strain: An International*
220 *Journal for Experimental Mechanics*. 2010;47 (3):227-240.
- 221 11. Vansovich K.A., Yadrov V.I., Beseliya D.C.. The Effect of Stress State Characteristics on the Surface Fatigue Cracks Growth
222 Rate Taking into Account Plastic Deformations. *Procedia Engineering*. 2015;113:244 - 253.
- 223 12. Clàudio R.A., Reis L., Freitas M.. Biaxial high-cycle fatigue life assessment of ductile aluminium cruciform specimens.
224 *Theoretical and Applied Fracture Mechanics*. 2014;73:82 - 90.
- 225 13. Misak H.E., Perel V.Y., Sabelkin V., Mall S.. Biaxial tension fatigue crack growth behavior of 2024-T3 under ambient air
226 and salt water environments. *Engineering Fracture Mechanics*. 2014;118:83-97.
- 227 14. Zhang Xin-Yan, Li Shu-Xin, Liang R., Akid R.. Effect of corrosion pits on fatigue life and crack Initiation. In: Proceedings
228 of 13th International conference on Fracture; June 16-21, 2013.
- 229 15. Schönbauer Bernd M., Stanzl-Tschegg Stefanie E.. Influence of environment on the fatigue crack growth behaviour of 12%
230 Cr steel. *Ultrasonics*. 2013;53(8):1399-1405.
- 231 16. Pfeil L.B.. The effect of occluded hydrogen on the tensile strength of iron.. *Proceedings of the Royal Society of London A*.
232 1926;112:128-195.
- 233 17. Beachem C.D.. A new model for hydrogen assisted cracking (hydrogen embrittlement).. *Metallurgical Transactions A*.
234 1972;3:437-451.
- 235 18. Misak H.E., Perel V.Y., Sabelkin V., Mall S.. Corrosion fatigue crack growth behavior of 7075-T6 under biaxial
236 tension-tension cyclic loading condition. *Engineering Fracture Mechanics*. 2013;106:38-48.
- 237 19. Perel V. Y., Misak H. E., Mall S., Jain V. K.. Biaxial Fatigue Crack Growth Behavior in Aluminum Alloy 5083-H116 Under
238 Ambient Laboratory and Saltwater Environments. *Journal of Materials Engineering and Performance*. 2015;24(4):1565-
239 1572.
- 240 20. Gaur V., Doquet V., Persent E., Mareau C., Roguet E., Kittel J.. Surface versus internal fatigue crack initiation in steel:
241 Influence of mean stress. *International Journal of Fatigue*. 2016;82 (3):437-448.
- 242 21. Gaur Vedit, Doquet Véronique, Persent Emmanuel, Roguet Eléonore. Effect of biaxial cyclic tension on the fatigue life and
243 damage mechanisms of Cr-Mo steel. *International Journal of Fatigue*. 2016;87:124-131.
- 244 22. Hénaff G., Petit J., Bouchet B.. Environmental influence on the near-threshold fatigue crack propagation behaviour of a high
245 strength steel. *International Journal of Fatigue*. 1992;14 (4):211-218.
- 246 23. Ritchie R.O.. Influence of impurity segregation on temper embrittlement and on slow fatigue crack growth and threshold
247 in 300-M high strength steel, *Met. Trans.* 8A, 1977, 1131-39. *Metallurgical Transactions A*. 1977;8:1131-1139.
- 248 24. Islam M.A., Bowen P., Knott J.F.. Intergranular fracture on fatigue fracture surface of 2.25Cr-1Mo steel at room temperature.
249 *Journal of Materials Engineering and Performance*. 2005;14 (1):28-36.
- 250 25. Stewart A.T.. The influence of environment and stress ratio on fatigue crack growth at near threshold stress intensities in
251 low-alloy steels. *Engineering Fracture Mechanics*. 1980;13:463-478.
- 252 26. Oriani R.A., Josephic P.H.. Equilibrium aspects of hydrogen-induced cracking of steels. *Acta Metallurgica*. 1974;22:1065-
253 1074.
- 254 27. Newman Jr J.C., Raju I.S.. An empirical stress-intensity factor equation for the surface crack. *Engineering Fracture*
255 *Mechanics*. 1981;15:185-192.



TABLE 1 Measured chemical composition of the Cr-Mo steel (wt. %).

| C | Cr | Mo | O | Mn | Si | Ni | Cu |
|----------|-----------|-----------|----------|-----------|-----------|-----------|-----------|
| 3.5 | 2.5 | 1.1 | 1.4 | 0.6 | 0.2 | 0.1 | 0.1 |

TABLE 2 Measured tensile properties of the steel at strain rate of 10^{-3} /sec

| Young's Modulus | Poisson's Ratio | Proportional Limit | 0.2% Yield stress | Ultimate Tensile stress | Vickers Hardness (HV 300) |
|------------------------|------------------------|---------------------------|--------------------------|--------------------------------|----------------------------------|
| 207 GPa | 0.27 | 600 MPa | 694 MPa | 780 MPa | 267 |

TABLE 3 Biaxial cyclic tension fatigue life data in air at $R = 0.25$, $\sigma_{zz,a}$ is the applied axial stress amplitude and B is the biaxiality ratio.

| $\sigma_{zz,a}$, MPa | B | Cycles to failure, N_f | Initiation location | Crack orientation |
|-----------------------|----------|--|----------------------------|--------------------------|
| 273 | 0 | 234,213 | Inner surface | Transverse |
| 265 | 0 | 258,366 | Outer surface | Transverse |
| 250 | 0 | 336,596 | Outer surface | Transverse |
| 280 | 0.25 | 115,531 | Outer surface | Transverse |
| 275 | 0.25 | 114,701 | Inner surface | Transverse |
| 270 | 0.25 | 129,972 | Inner surface | Transverse |
| 270 | 0.25 | 1,908,883 | Inner surface | Transverse |
| 268 | 0.25 | 219,697 | Inner surface | Transverse |
| 265 | 0.25 | > 3,000,000 | - | - |
| 255 | 0.25 | > 3,000,000 | - | - |
| 287 | 0.5 | 302,091 | Outer surface | Transverse |
| 280 | 0.5 | > 3,000,000 | - | - |
| 275 | 0.5 | > 3,000,000 | - | - |
| 270 | 0.5 | 238,224 | Outer surface | Transverse |
| 270 | 0.5 | 296,839 | Outer surface | Transverse |
| 265 | 0.5 | 145,221 | Outer surface | Transverse |
| 260 | 0.5 | > 3,000,000 | - | - |
| 270 | 1 | 65,424 | Inner surface | Longitudinal |
| 260 | 1 | 143,084 | Inner surface | Longitudinal |
| 250 | 1 | 645,832 | Outer surface | Longitudinal |
| 247 | 1 | 160,916 | Outer surface | Longitudinal |
| 245 | 1 | 227,250 | Inner surface | Transverse |
| 242 | 1 | > 3,000,000 | - | - |
| 235 | 1 | > 3,000,000 | - | - |

TABLE 4 Corrosion fatigue data without cathodic potential under uniaxial ($B = 0$) and equibiaxial ($B = 1$) tension at $R = 0.25$. $\sigma_{zz,a}$ is the applied axial (or longitudinal) stress amplitude and B is the load biaxiality ratio.

| $\sigma_{zz,a}$, MPa | B | Cycles to failure, N_f | Initiation location | Crack orientation |
|-----------------------|-----|--------------------------|---------------------|--|
| 240 | 0 | 146,333 | Outer surface | Transverse |
| 220 | 0 | 140,797 | Outer surface | Transverse |
| 210 | 0 | 194,558 | Outer surface | Transverse |
| 195 | 0 | 363,411 | Outer surface | Transverse |
| 180 | 0 | 154,735 | Outer surface | Transverse |
| 155 | 0 | 524,377 | Outer surface | Transverse |
| 235 | 1 | 155,831 | Outer surface | Longitudinal |
| 220 | 1 | 164,753 | Outer surface | Inclined crack 15° with longitudinal direction |
| 210 | 1 | 198,505 | Outer surface | Longitudinal |
| 195 | 1 | 266,320 | Outer surface | Inclined crack 69° with longitudinal direction |
| 180 | 1 | 304,076 | Outer surface | Inclined crack 80° with longitudinal direction |
| 155 | 1 | 586,777 | Outer surface | Inclined crack 58° with longitudinal direction |

TABLE 5 Corrosion fatigue data with cathodic potential for different load biaxiality ratios at $R = 0.25$. $\sigma_{zz,a}$ is the applied axial (or longitudinal) stress amplitude and B is the load biaxiality ratio.

| $\sigma_{zz,a}$, MPa | B | Cycles to failure, N_f | Initiation location | Crack orientation |
|-----------------------|------|--------------------------|---------------------|-------------------|
| 270 | 0 | 165,675 | Outer surface | Transverse |
| 262 | 0 | 187,877 | Outer surface | Transverse |
| 250 | 0 | > 3,000,000 | - | - |
| 278 | 0.25 | 81,012 | Outer surface | Transverse |
| 270 | 0.25 | 603,263 | Inner surface | Transverse |
| 260 | 0.25 | > 3,000,000 | - | - |
| 265 | 1 | 145,296 | Inner surface | Transverse |
| 244 | 1 | 455,176 | Outer surface | Longitudinal |

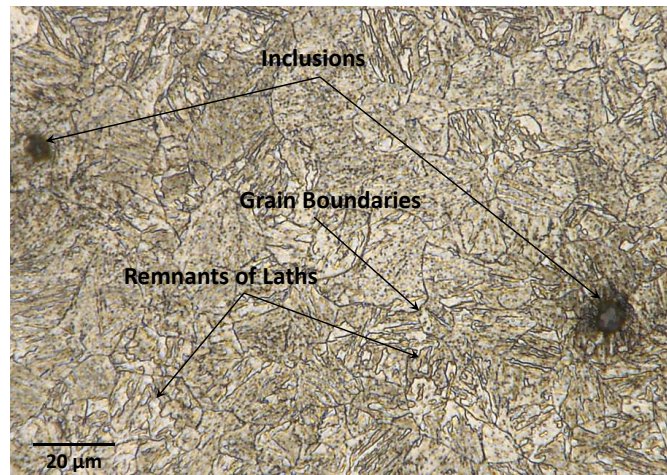


FIGURE 1 Microstructure of the Cr-Mo steel.

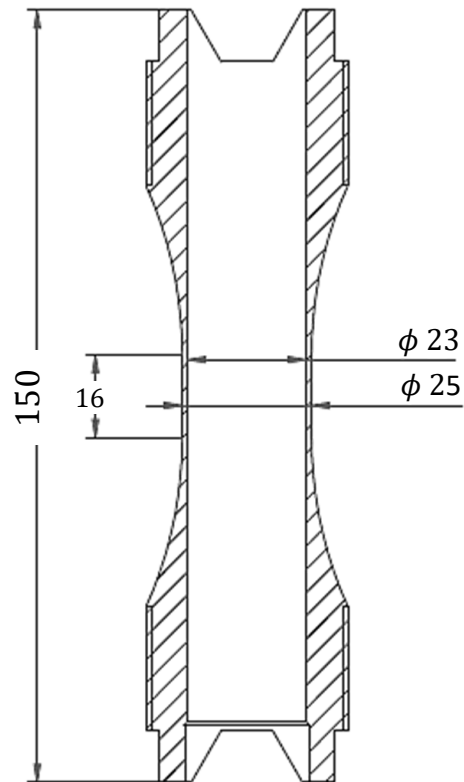


FIGURE 2 Geometry of tubular specimen used for biaxial tension fatigue tests.

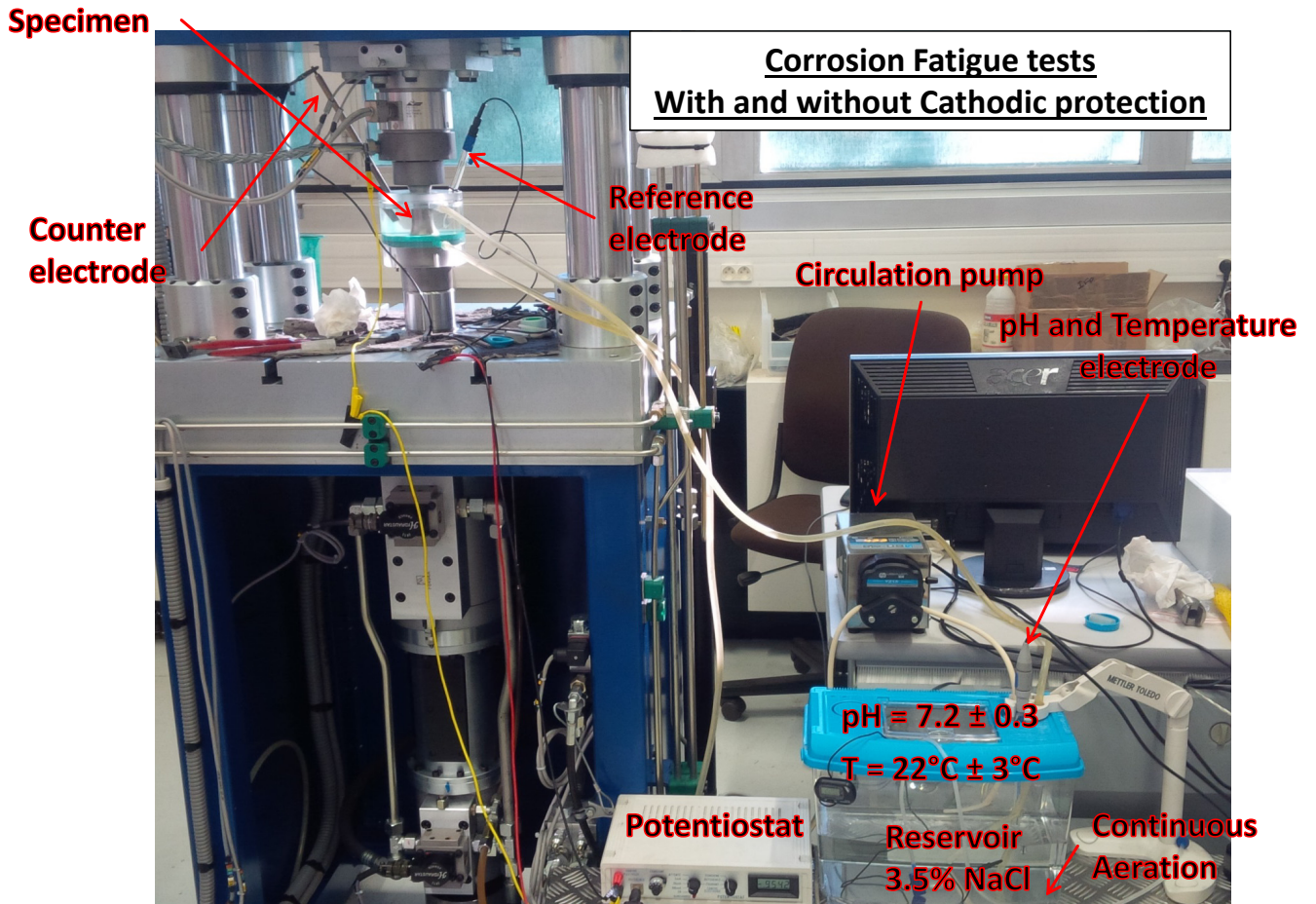


FIGURE 3 Experimental setup designed in lab to simulate corrosion fatigue tests.

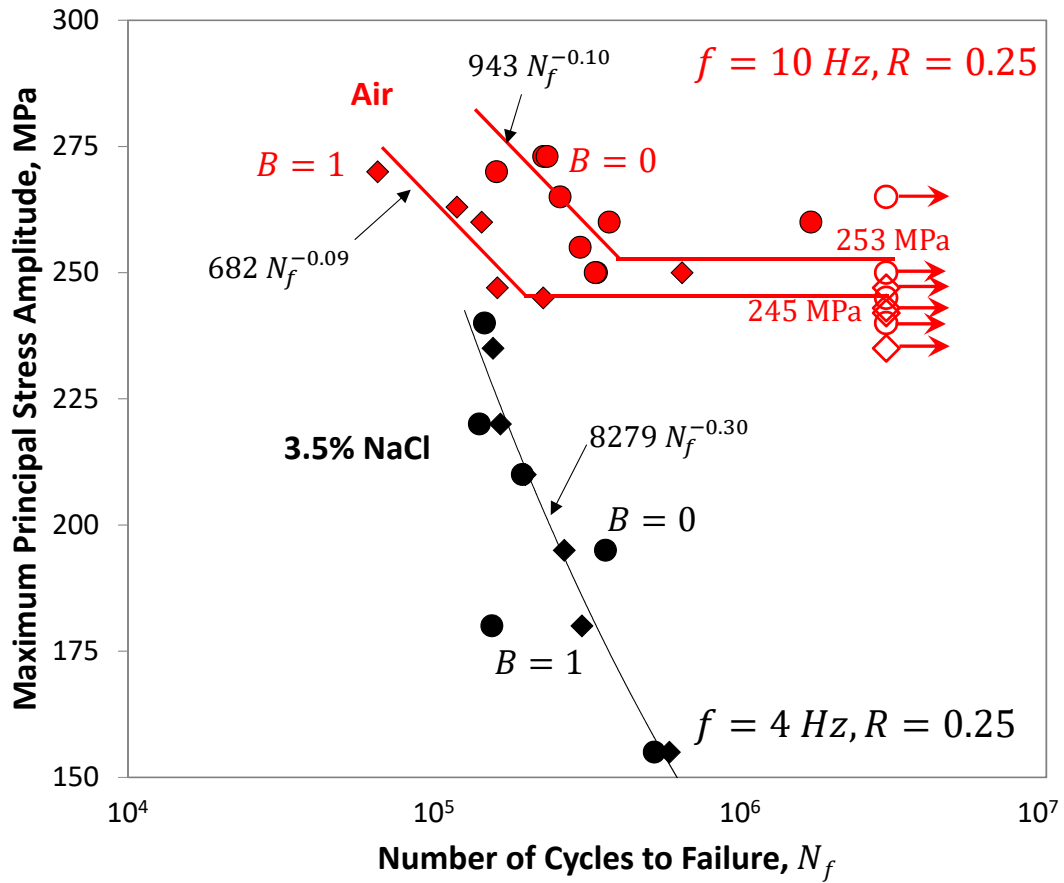


FIGURE 4 S-N curve for uniaxial ($B=0$), circular symbol and biaxial tension ($B=1$), diamond symbol, in air (red) and in salt water (black).

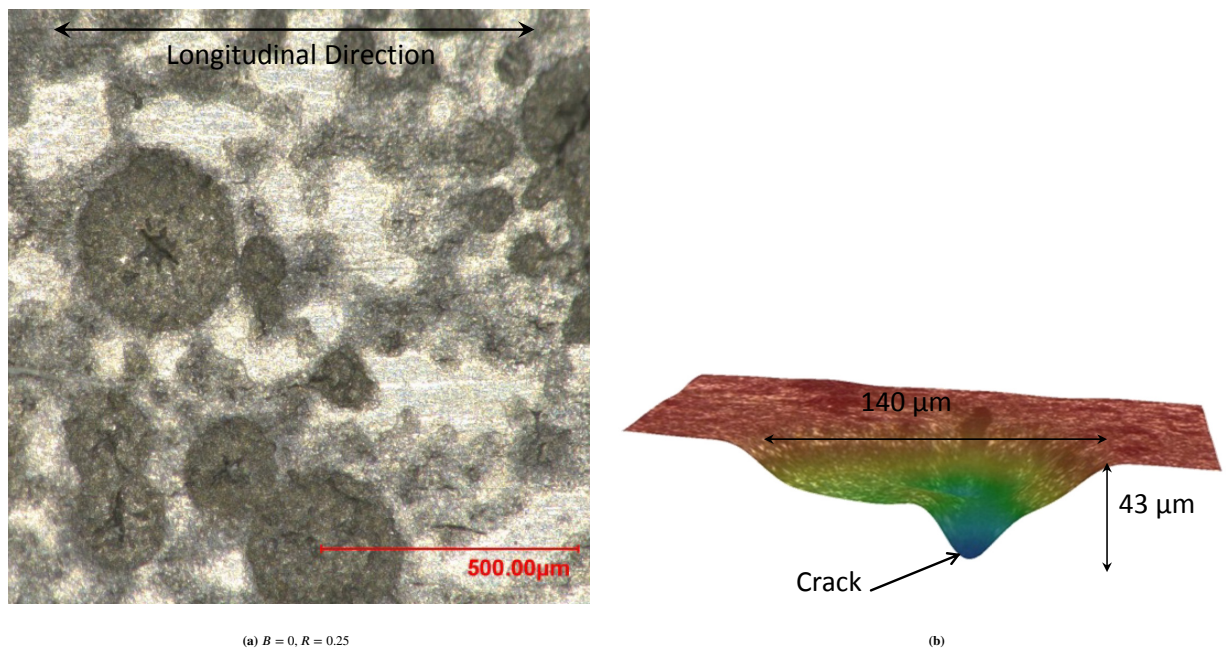


FIGURE 5 (a) An example of formation of corrosion pits during corrosion fatigue tests, (b) A 3D topographic image of a typical micro-pit observed on corroded surface after fatigue test.

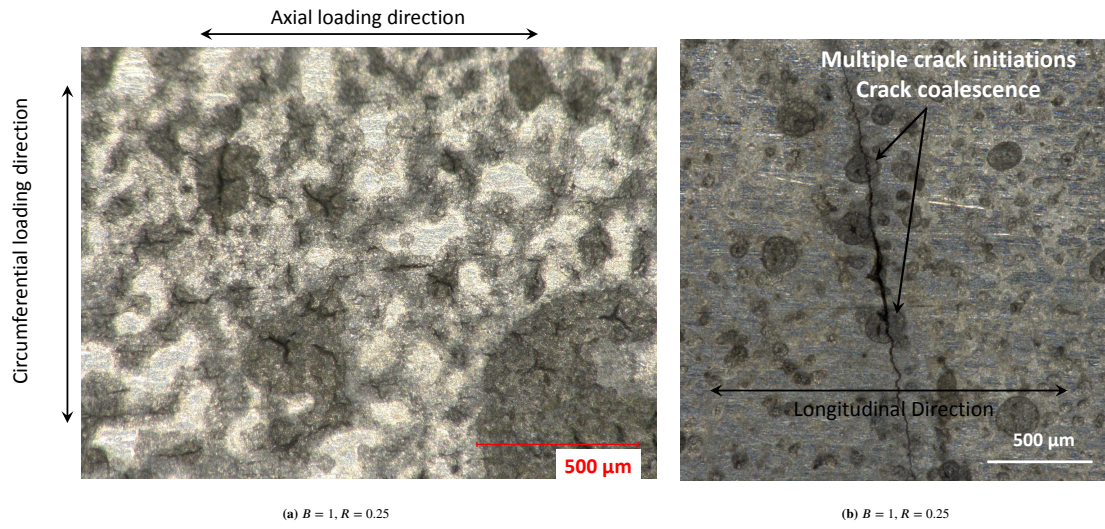


FIGURE 6 (a) An example of randomly oriented micro-cracks under equibiaxial tension and, (b) merging of several small crack from micro-pits leading to a macro crack.

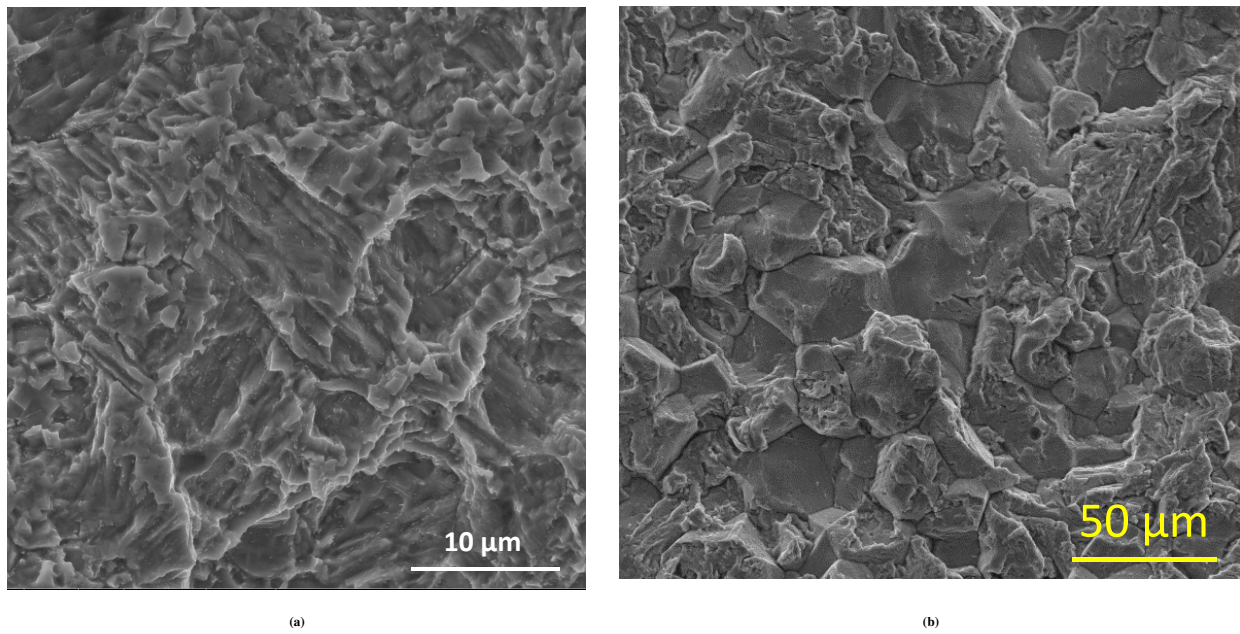


FIGURE 7 SEM image of fracture surface in salt water (a) uniaxial tension at $\sigma_a = 155$ MPa. (b) biaxial tension $\sigma = 210$ MPa, depicting the micro-pits, mixed intergranular and brittle decohesion type features.

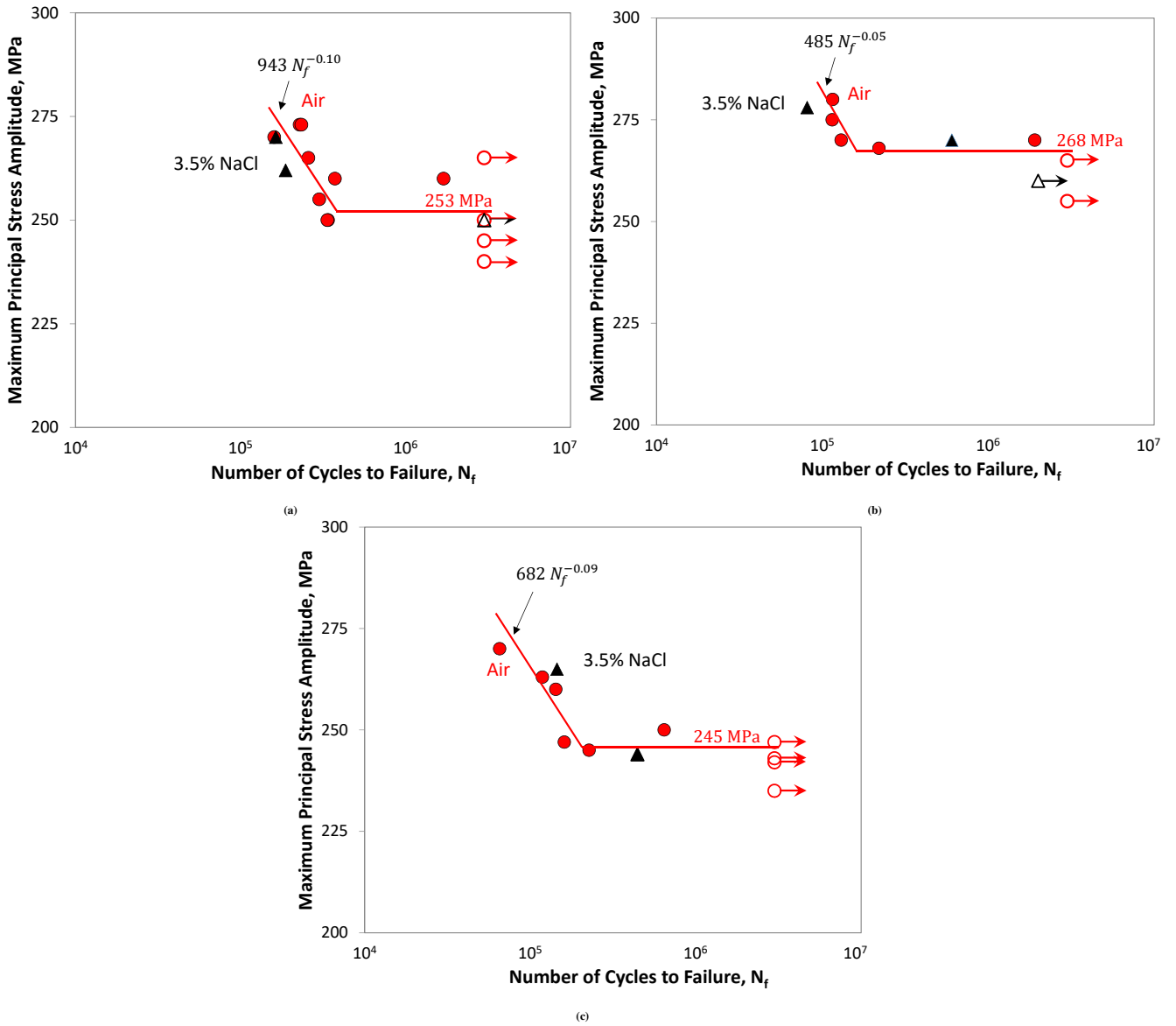


FIGURE 8 S-N curves for fatigue data in air and in salt water with cathodic potential for different load biaxiality ratios: (a) $B = 0$, (b) $B = 0.25$ and (c) $B = 1$. Hollow symbols represent ran-out specimens.

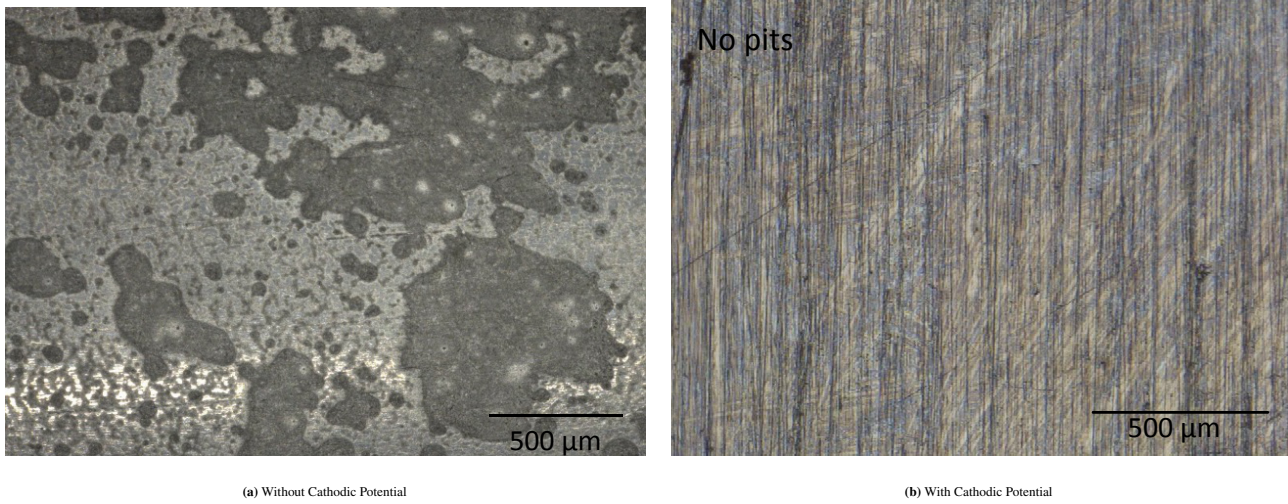


FIGURE 9 Comparison of surface condition after fatigue tests in salt water with and without cathodic potential.

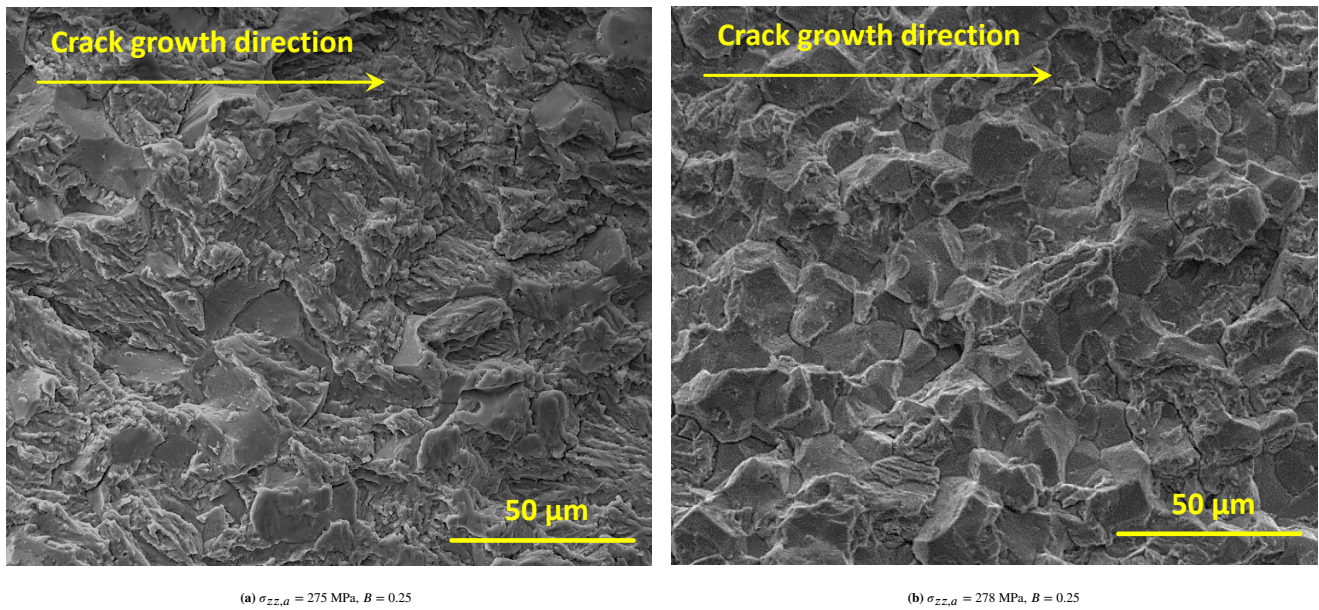


FIGURE 10 A SEM image of fracture surface at nearly same ΔK and magnification in (a) air and (b) salt water with cathodic potential.

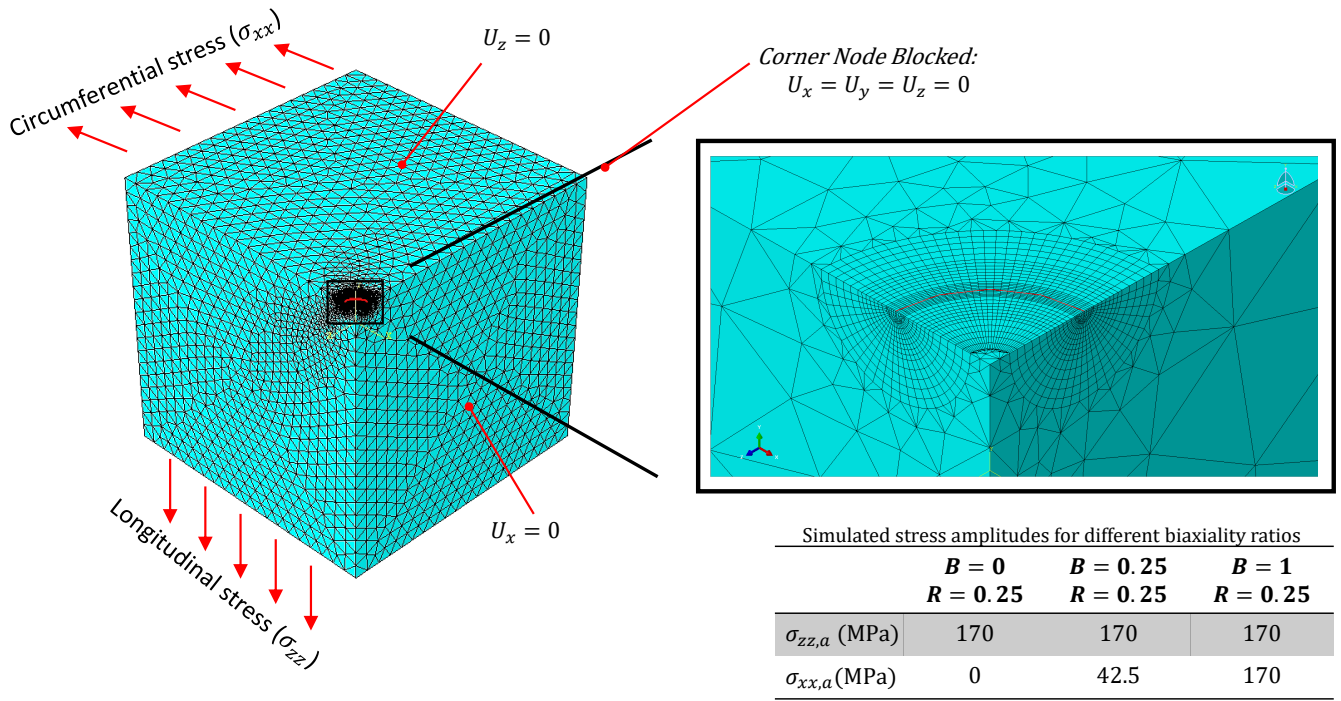


FIGURE 11 FE mesh of a model containing 500 μm semi-circular surface crack with applied boundary conditions.

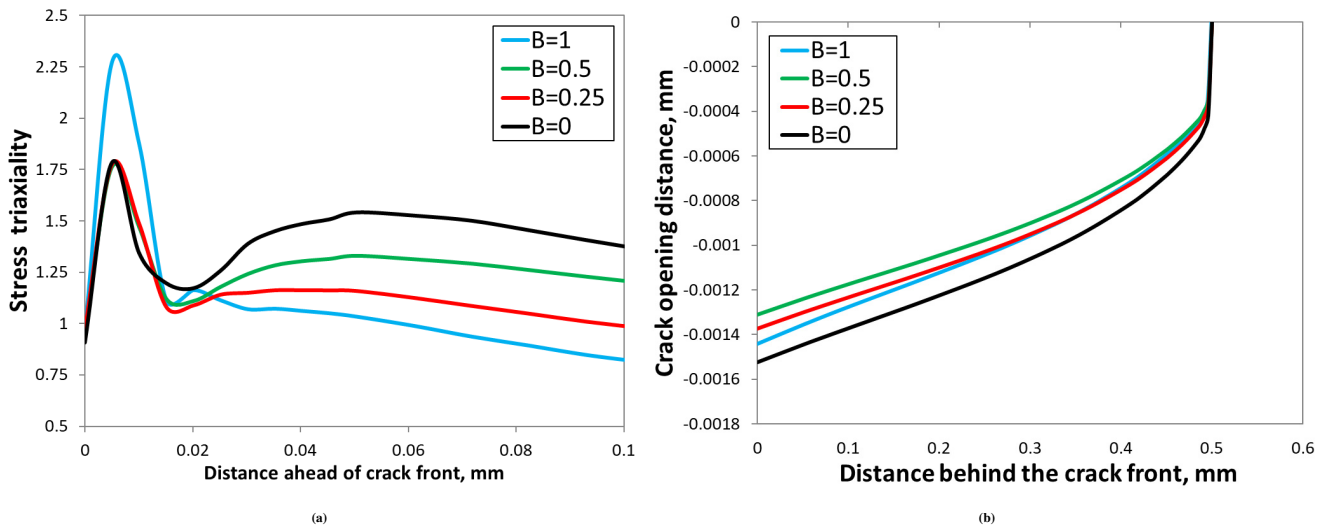


FIGURE 12 (a) Profile of stress triaxiality ratio ahead of the crack front for different load biaxiality ratios and (b) Profile of crack opening displacement behind the crack front for different load biaxiality ratios.